CHAPTER 5

IMPACT OF HIGH-PRESSURE MICROFLUIDIZATION TREATMENT ON THE PROPERTIES OF BACTERIAL CELLULOSE DERIVED FROM THAI RED TEA KOMBUCHA

5.1 Abstract

This study investigates the effect of high-pressure microfluidization (HPM) on the characteristics of bacterial cellulose (BC) produced from optimized Thai red tea formulations. BC was purified, blended, and subjected to HPM at 10,000 Psi for 10, 15, and 20 cycles. The treatment significantly altered BC properties, reducing moisture content (96.85%–98.96%) and water-holding capacity (WHC), with untreated BC (96.58 ± 13.91 g/g) exhibiting higher WHC than HPM-treated samples (30.93 ± 3.05–31.04 ± 3.18 g/g). Fiber diameter decreased with increased HPM cycles, from 37 nm (untreated) to 24.99 nm (BCH-20-FD), especially in freeze-dried samples. Particle size analysis showed smaller, more uniform particles post-HPM, though polydispersity index and zeta potential indicated partial re-aggregation. Scanning electron microscopy (SEM) and X-ray diffraction (XRD) confirmed morphological and crystallinity changes, with freeze-drying enhancing fibril refinement and porosity, while oven-drying yielded denser structures. Thermogravimetric analysis (TGA) indicated reduced thermal stability in freeze-dried BC. These findings highlight HPM and drying as key factors influencing BC's physical, structural, and thermal properties, offering adaptable strategies for optimizing BC in various applications.

Keywords: Thai red tea, bacterial cellulose, high-pressure microfluidic, BC properties, freeze drying

5.2 Introduction

BC is a unique biopolymer distinguished by its high purity, biocompatibility, flexibility, nano-porosity, and biodegradability, setting it apart from plant-derived cellulose (Hussain et al. 2019; Yilmaz and Goksungur 2024). These attributes have led to its wide application across various industries, including food, packaging, cosmetics, biomedical, pharmaceutical, textiles, and electronics (Hussain et al. 2019; Zhong 2020; Choi et al. 2022). Its nanofibrillar network provides an excellent platform for developing advanced functional materials, particularly when modified through post-production treatments.

Although BC exhibits impressive native properties, its structure often requires further modification to meet the demands of specific industrial applications. High-pressure techniques such as high-pressure homogenization (HPH) and high-pressure microfluidization (HPM) have emerged as effective physical treatments for altering cellulose morphology. These methods apply intense shear forces under high pressure to reduce particle and fiber sizes, improving functionality (Wang et al. 2015; Mert 2020). Notably, HPM differs from HPH in its use of a specialized interaction chamber with microchannels, allowing for finer and more uniform particle breakdown through combined shear, impact, and cavitation forces (Guo et al. 2020).

Several studies have investigated the use of HPH and HPM to alter the structure and properties of cellulose, including BC. These treatments can modify critical characteristics such as fiber diameter, crystallinity index, and thermogravimetric properties, demonstrating significant potential for diverse applications (Wang et al. 2015, 2019a; Li et al. 2020; Suryanto et al. 2021; Muhajir et al. 2022). Specifically, HPH has been shown to reduce the crystallinity index and porosity of BC, especially at higher pressures (Muhajir et al. 2022). The number of HPH cycles is a critical factor influencing BC properties, affecting film tensile strength, surface roughness, porosity, crystallinity index, and crystallite size (Suryanto et al. 2021). Adjusting processing parameters such as pressure levels, number of cycles, and initial BC characteristics can

further refine BC properties. Increasing the number of HPH cycles progressively decreases fiber size, modifies crystallinity, and increases surface area, thereby influencing properties like water-holding capacity, mechanical strength, and rheological behavior (Suryanto et al. 2021; Muhajir et al. 2022). While HPH has been extensively studied, particularly for plant-based cellulose, research on the effects of HPM on BC properties remains limited.

This study aims to address this gap by investigating the impact of high-pressure microfluidization on BC produced from Thai red tea kombucha. Building on a previously optimized fermentation formula, the research evaluates structural and functional changes in BC under varying HPM conditions. The findings aim to contribute to the development of post-processing strategies that enhance BC's applicability across multiple sectors.

5.3 Materials and Methods

The materials and equipment used in this study include commercial kombucha starter (SCOBY) bought from Neo Cold Brew Shop (online market, Thailand), Thai red tea-vanila flavor *ChaTraMue* brand (RTC), commercial white sugar (sucrose), glucose, ethanol, sodium hydroxide (NaOH, Merck), Reverse osmosis (RO) water, Deionized (DI) water, cheesecloth, coffee filter, glass jar, funnel, autoclave, laboratory glassware, laminar air flow, analytical balance (Mettler Toledo), incubator, pH-meter (Oakton, pH 700), refractometer, Electric-Hydraulic Microfluidizer Processor Homogenizer (M-110EH-30, Microfluidics, USA), centrifugal machine (Avanti JXN-26, Beckman Coulter, USA), Oven dryer (XUE058, FRANCE ETUVES), freeze dryer (SJ-10N-60A Vacuum Freeze Dryer), FT-IR (Bruker VERTEX 70), XRD (Bruker D8 Advance), SEM/FESEM (Zeiss, AURIGA, Germany), TGA-instrument, and nano particle size and zeta potential analyzer (Malvern/Zetasizer-ZS).

5.3.1 Bacterial Cellulose Production

1) Medium Preparation and Fermentation

BC production was carried out based on the procedure outlined in the previous chapter (Chapter 3), using the optimized medium formula (RTC-V1) identified as the most suitable. The medium for Thai red tea kombucha fermentation consists of 7.97% (w/v) sucrose, 2.03% (w/v) glucose, 1.41% (w/v) Thai red tea, and 1.60% (v/v) ethanol, with a final volume of 2 to 4 liters per batch. The fermentation vessel was a plastic box measuring 44 x 31 x 12 cm (length x width x height).

Prior to BC production, an inoculum was prepared, comprising 10% (v/v) of the total fermentation medium. The inoculum was prepared using the RTC-C formula, which included 10% (w/v) sucrose and 1% (w/v) Thai red tea, inoculated with 10% of the culture from the previous fermentation, and incubated for 14 days. For medium preparation, sucrose and glucose were added to a 5L Duran bottle. Thai red tea was brewed with hot deionized water (approximately 90°C) to around 60% of the final volume for 15 minutes. The tea was then filtered using coffee filter paper, and the volume was recorded. The residue was further rinsed with a small amount of hot deionized water (approximately 90°C) and shaken for about 1 minute to complete the extraction, achieving a final volume of tea extract equal to 80% of the total volume. The tea extract was then poured into the Duran bottle with sucrose and glucose and mixed well. The solution was sterilized by autoclaving at 121°C and 1 psi for 15 minutes. After sterilization, the medium was allowed to cool to room temperature (35–40°C) before being inoculated with the prepared inoculum. The medium was carefully shaken, transferred from a 5 L Duran bottle to a plastic box, and fermented for 15 days at 30°C.

2) BC Harvesting and Purification

After 15 days of fermentation, the BC was carefully removed from the fermentation batch. The BC was then cut into small pieces, approximately 2 x 2 x 2 cm, depending on its thickness. The sample was boiled in water for 30 minutes,

drained for 10 minutes, and treated with a 2% NaOH solution at approximately 90°C for 120 minutes to remove impurities. Following this, the BC was thoroughly rinsed with reverse osmosis (RO) water and soaked in RO water with frequent changes until the pH became neutral (Yanti et al. 2018; Aswini et al. 2020). The purified BC was then stored for further processing and analysis.

5.3.2 Bacterial cellulose nanofibrilation

The purified BC slice was crushed using a blender. Approximately 250 grams of BC (wet weight) were placed in a blender, mixed with RO water at a ratio of 1:2, and ground for about 10 minutes. BC suspension was then separated using a stainless-steel strainer with a mesh size of approximately 2 x 2 mm. The resulting filtrate suspension was used for high-pressure micro-fluidization (HPM) treatment.

To investigate the effects of HPM, approximately 3000 ml of the BC suspension was processed using a high-pressure microfluidizer (M-110EH-30, Microfluidics, USA) at 10,000 psi for varying cycles: 10 cycles (BCH-10), 15 cycles (BCH-15), and 20 cycles (BCH-20). The resulting BC nanofibers (BCNFs)/BCH were separated by centrifugation at 6000 rpm for 30 minutes at 25°C using a centrifuge (Avanti JXN-26, Beckman Coulter, USA). A sample of the BC suspension without HPM treatment was also centrifuged under the same conditions and labeled as BCP (BC-pulp). The sample of BCP and BCH were stored in jars at a temperature of 4–6°C. For analysis, some of the BCNFs samples were dried using two different methods: oven drying at 40°C and freeze-drying.

5.3.3 Characterization of BC and BCNFs

1) Moisture Content and WHC

The WHC of the samples was determined by drying the purified BC and BCNFs samples. For BC, approximately one slice of purified samples weighing about 10 grams per slice was used, while for BC pulp and BC-HPM, around 5.00 grams (wet weight) of samples were prepared. All samples were dried in an oven at 40°C until a constant dry weight was achieved. The measurements were performed in triplicate,

and the moisture content and WHC were calculated using Equations below (**Eq. 5.1 and Eq. 5.2**).

$$Moisture\ content = \frac{wet\ wight - dry\ weight}{wet\ weight}\ x\ 100\% \quad \text{.....(Eq. 5.1)}$$

$$WHC = \frac{wet\ wight - dry\ weight}{dry\ weight} \quad \text{.....(Eq. 5.2)}$$

2) Characterization of BC Particles

BC-pulp and BC-HPM samples were prepared for particle size analysis by dispersing them 50 times. Specifically, 1 gram of each sample was diluted in a 50 ml volumetric flask with deionized (DI) water. The sample was stirred at 300 rpm for 15 minutes, sonicated for 10 minutes, and then stirred again for 10 minutes. The size distribution of nanoparticles was measured using a Malvern Zetasizer Nano ZS (Malvern Instruments Ltd., UK) employing the dynamic light scattering (DLS) technique. The parameters for the BC sample were set to an absorption of 0.0000 and a refractive index of 1.618, while the dispersant (water) parameters were set to a refractive index of 1.330 and a viscosity of 0.8882 cP. The analysis was performed at a temperature of 25°C, using a disposable sizing cuvette, with a measurement duration of 60 seconds and a measurement position of 4.65 mm. The size distribution graphs were recorded.

The samples were diluted 100 times for zeta potential analysis and prepared using the same procedure as for particle size analysis. The dispersant (water) parameters were set to a refractive index of 1.330, a viscosity of 0.8872 mPa.s, and a dielectric constant of 78.5. The analysis was conducted at a temperature of 25°C using a zeta dip cell, with 12 zeta runs and a measurement position of 4.5 mm.

3) Other Characterization of BC

Additional characterization of BC was performed using SEM, FTIR, XRD, and TGA. The detailed methods and procedures for these analyses are provided in **Chapter 3** of this thesis.

5.3.4 Statistical Analysis

Analysis of variance was carried out using Ms. Excel software. The differences between the mean values were analyzed using least significant difference (LSD) test and the significance level was set at $P < 0.05$.

5.4 Results and Discussion

5.4.1 Moisture Content and Water Holding Capacity

The moisture content and water-holding capacity (WHC) of the BC samples, including purified BC sheets (BCC), centrifuged blended BC suspensions (BCP), and centrifuged microfluidized BC suspensions (BCH-10, BCH-15, and BCH-20), are summarized in **Table 5.1.**

Table 5.1 Moisture content and WHC of BC pulp and microfluidized BC

Samples	Moisture content (%)	WHC (g water/g cellulose)
BCC	98.96±0.15	96.58±13.91
BCP	97.60±0.11	40.70±1.93
BCH-10	96.85±0.32	30.93±3.05
BCH-15	96.86±0.24	31.01±2.53
BCH-20	96.87±0.21	31.04±2.21

The moisture content of the samples ranged from 96.85% to 98.96%. BCC exhibited the highest moisture content (98.96±0.15%), indicating its high capacity to retain water in its purified sheet form. In contrast, BCP, a centrifuged BC suspension, had slightly lower moisture content (97.60±0.11%), likely due to partial dehydration during the centrifugation process. The microfluidized BC samples (BCH-10, BCH-15, BCH-20) showed the lowest moisture content, ranging from 96.85% to 96.87%.

The reduction in moisture content in BCP and microfluidized samples can be attributed to mechanical processes such as blending and HPM. The blending process applies mechanical shear forces that partially disrupt the cellulose network,

reducing its ability to retain water. HPM further intensifies this structural disruption, leading to enhanced water release. Additionally, the centrifugation process expels loosely bound water through centrifugal force. Similar effects of mechanical processing on cellulose structure and water retention have been reported (Betlej et al. 2021). Despite these reductions, the high overall moisture content in all samples reflects the inherently hydrophilic nature of BC, attributed to its porous, three-dimensional network structure (Fang and Catchmark 2014; Gayathry and Gopalaswamy 2014; R. Rebelo et al. 2018; Widyastuti and Kartika Fitri 2023). Variations in moisture content among the samples underscore the significant role of processing techniques in modulating BC's water retention properties.

WHC values showed significant variation among the samples, ranging from 96.58±13.91 g water/g cellulose in BCC to 30.93±3.05 g water/g cellulose in BCH-10. BCC demonstrated the highest WHC, reflecting its intact, undisturbed network structure in sheet form, which can trap and retain a large amount of water. On the other hand, BCP, with a WHC of 40.70±1.93 g water/g cellulose, exhibited a lower capacity due to partial disruption of the network due to the centrifugation, which reduced the size of BC, its porosity, and water retention ability. The microfluidized BC samples (BCH-10, BCH-15, BCH-20) showed the lowest WHC, approximately 30.93–31.04 g water/g cellulose. This significant reduction in WHC can be attributed to the microfluidization process, which breaks down the cellulose fibers into smaller fragments and disrupts the interconnected network. The mechanical forces during homogenization reduce porosity and the surface area available for water entrapment (Suryanto et al. 2021; Muhajir et al. 2022; Tomkowiak et al. 2024). The similarity in WHC values among the microfluidized samples suggests that the degree of microfluidization (10, 15, or 20 passes) had minimal additional impact on WHC beyond the initial disruption caused by the process.

5.4.2 Particle Analysis

The particles of BCP and microfluidized BC samples were analyzed for particle size distribution, polydispersity index, and zeta potential. The results of the particle analysis are summarized in **Table 5.2**, with the particle size distribution also visualized in graphical form (**Figure 5.1**).

Table 5.2 Results of polydispersity index analysis of BC from different mechanical treatments

Samples	diameter average (nm)			% intensity			PDI	ZP (mV)
	peak 1	peak 2	peak 3	peak 1	peak 2	peak 3		
BCP	4968.33	132.23	1.39	69.53	27.67	2.80	0.997	-14.133
	±208.80	±52.11	±2.41	±6.71	±3.21	±4.85	±0.01	±1.60
BCH-10	4570.67	253.80	25.63	51.83	37.23	8.87	0.813	-5.830
	±177.39	±16.60	±11.95	±4.20	±1.84	±2.15	±0.09	±0.43
BCH-15	5501.67	248.90	19.62	28.07	62.37	9.77	0.993	-6.773
	±101.04	±20.87	±10.10	±1.77	±15.79	±1.46	±0.01	±0.167
BCH-20	247.43	34.81	10.07	58.53	33.90	7.57	0.935	-5.357
	±72.61	±26.59	±8.86	±0.64	±40.41	±1.74	±0.07	±0.94

BC suspensions showed significant differences in particle size distribution between non-microfluidized (BCP) and microfluidized (BCH) samples. BCP exhibited a broad size distribution with large aggregates (4968.33 ± 208.80 nm) and smaller peaks (132.23 ± 52.11 nm and 1.39 ± 2.41 nm), indicating high polydispersity. Micro-fluidized samples showed progressive size reductions: BCH-10 had peaks at 4570.67 ± 177.39 nm, 253.80 ± 16.60 nm, and 25.63 ± 11.95 nm; BCH-15 had peaks at 5501.67 ± 101.04 nm, 248.90 ± 20.87 nm, and 19.62 ± 10.10 nm; BCH-20 showed the most significant reduction with peaks at 247.43 ± 72.61 nm and smaller peaks dominating the distribution. These results confirm that high-pressure, especially HPM, effectively reduces BC aggregates, producing smaller, more uniform particles,

consistent with previous studies on biopolymer suspensions (Suryanto et al. 2021; Muhajir et al. 2022).

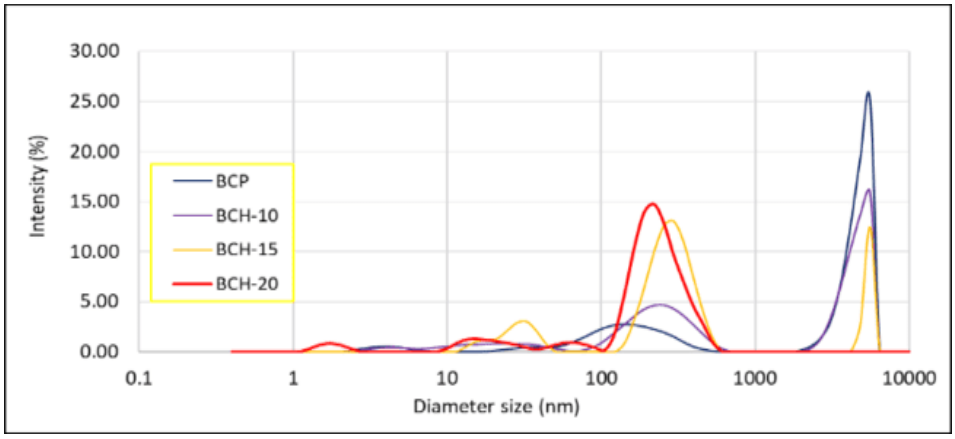

Figure 5.1 Graph of poly distribution particle size from BC-Pulp and microfluidized BC suspension

The polydispersity index (PDI) further supports these observations. The BCP sample exhibited a PDI of 0.997 ± 0.01, confirming its highly polydisperse nature. With microfluidization, the PDI values decreased, indicating improved uniformity in particle size distribution. BCH-10 had a PDI of 0.813 ± 0.09, reflecting the reduction in size variability. However, BCH-15 showed a slight increase in PDI to 0.993 ± 0.07, likely due to the dominance of a large primary peak alongside smaller peaks, suggesting partial re-aggregation during processing. BCH-20 exhibited a PDI of 0.935 ± 0.07, indicating a relatively uniform size distribution compared to BCP but still reflecting a polydisperse system. The PDI value ranges from 0.0, indicating a perfectly uniform sample in terms of particle size, to 1.0, representing a highly polydisperse sample with a wide range of particle size populations (Danaei et al. 2018). A similar trend of the result was also reported in a study. Microfluidized BC with HPM in 1, 10, and 25 cycles has a PDI value of 1.000, 0.154, and 0.551 (Dima et al. 2017).

The ZP values provide insights into the stability of BC suspensions. The BCP sample exhibited a ZP of -14.133 ± 1.60 mV, indicating moderate stability due to limited electrostatic repulsion between particles. After microfluidization, BCH-10

showed a slight improvement to -5.830 ± 0.43 mV, while BCH-15 and BCH-20 had the ZP values of -6.773 ± 0.167 mV and -5.357 ± 0.94 mV, respectively. Despite significant size reduction, the relatively low ZP values across all samples indicate that microfluidization does not enhance suspension stability. A ZP of at least ±30 mV is typically required for high colloidal stability (Yan et al. 2016). For comparison, previous studies reported ZP values of -10.4, -10.2, and -13.1 mV for microfluidized BC after 1, 10, and 20 passes, respectively (Dima et al. 2017).

Information on the specific effects of HPM on the size, PDI, and zeta potential of BC remains limited in previous studies. However, some research has explored nanoparticle synthesis from BC using alternative methods. For instance, nanocellulose produced through a wet milling process followed by chemical and filtration treatments exhibited average particle sizes of 44.06 nm (peak 1), 132.1 nm (peak 2), and 637.4 nm (peak 3), with PDIs of 10.4%, 16.9%, and 12.8%, respectively (Nurfadila et al. 2019). Similarly, BC aqueous suspensions treated with HCl hydrolysis yielded BC nanoparticles (BCNPs) with average sizes of 590.9 nm and 221.4 nm for untreated and treated samples, respectively, PDIs of 0.37 and 0.18, and zeta potentials of −21.36 ± 3.32 mV and −39.50 ± 4.01 mV, respectively (Zhai et al. 2020). Additionally, BCNPs produced via shaking methods followed by alkaline treatment, dialysis, sonication with polysorbate 80 surfactant, and filtration through a 200 nm syringe filter showed a particle size of 478.9 ± 129.6 nm and a zeta potential of −14.1 ± 4.2 mV, closely matching values reported in this study (Balistreri et al. 2024).

In summary, HPM had variable effects on BC suspensions. BCH-20 demonstrated a significant reduction in particle size, indicating the effectiveness of HPM in breaking down aggregates. However, the PDI of BCH-15 and BCH-20 remained comparable to that of BCP, suggesting inconsistent improvements in size uniformity across the samples. Additionally, the low ZP values observed for all samples indicate limited electrostatic stabilization, pointing to poor suspension stability. These findings emphasize the need for further optimization, such as incorporating stabilizing agents,

surfactants, or pH adjustments, to enhance both the stability and functionality of BC suspensions, which are critical for their application in industrial and biomedical fields.

5.4.3 BC Morphology

The SEM images show the structural differences in BC sheets after various treatments (Figure 6.2). These include HPM at 10, 15, and 20 passes and two drying methods: oven-dried and freeze-dried. The non-microfluidized BC (BCP-O and BCP-FD) displays dense and compact fibril networks, with the freeze-dried sample showing slightly more porosity than the oven-dried sample. After microfluidization, BCH-10-O shows disrupted fibril arrangements, while BCH-10-FD has a more open and porous structure. In BCH-15 and BCH-20, higher microfluidization intensity causes finer and more fragmented fibril networks. Freeze-dried samples are consistently more porous and less compact than oven-dried ones, showing the drying method strongly affects the microstructure. The BCC samples, used as a control, demonstrate a well-preserved fibril network in the oven-dried state. These results highlight the significant influence of microfluidization intensity and drying methods on the BC microstructure. Higher microfluidization intensities lead to finer and more fragmented fibril networks, while freeze-drying, observed in other samples, promotes a more porous morphology. The result of this study is in accordance with the previous study on the effect of HPM (Suryanto et al. 2021; Muhajir et al. 2022) and on the effect of different drying method (Zhang et al. 2011; Andree et al. 2021; Mohamad et al. 2022b).

The SEM image analysis was further utilized to determine the fiber diameter of BC. The results are summarized in **Table 5.3**, while the graphs illustrating the fiber size distribution of BC are presented in **Figure 5.2.**

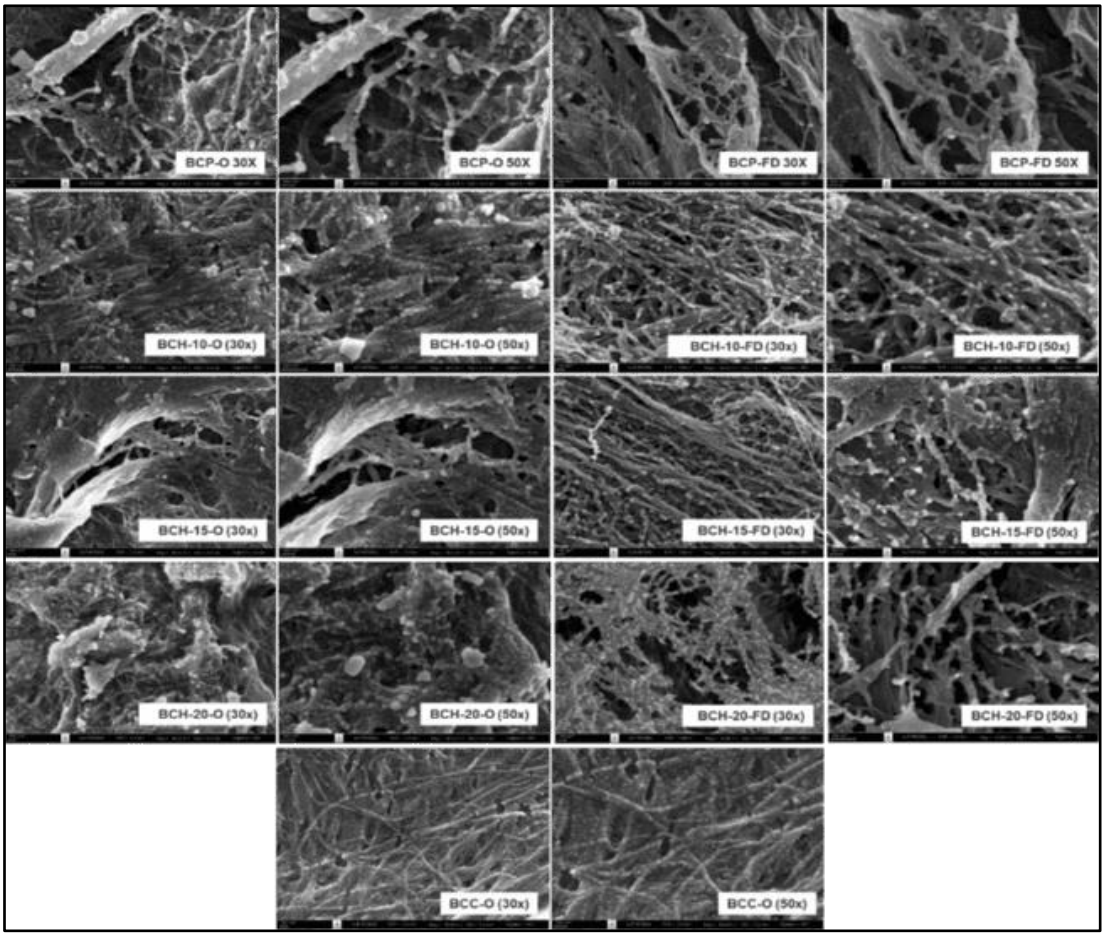

Figure 5.2 SEM image of BC sample BC sheet (BCC), BCP, HPM1, HPM2, dan HPM3. The symbol of O (oven drying), and FD (freeze dried)

Table 5.3 Resume of the diameter size of the dried BC samples with different mechanical treatment and drying methods.

	Diameter (nm)								
	Oven Dried (O)					Freez Dried (FD)			
	BC-C	BCP	BCH-10	BCH-15	BCH-20	BCP	BCH-10	BCH-15	BCH-20
Mean	37.00	37.15	31.61	30.57	26.72	33.26	31.33	26.71	24.99
Min.	26.65	23.80	18.87	23.32	19.24	24.67	22.28	18.78	16.49
Max.	51.24	53.76	46.75	45.24	35.06	46.30	39.68	39.78	39.24
Sd	4.77	7.18	6.38	4.55	3.92	5.17	4.46	4.06	3.98

Min = minimum, Max = maximum, Sd = standard deviation

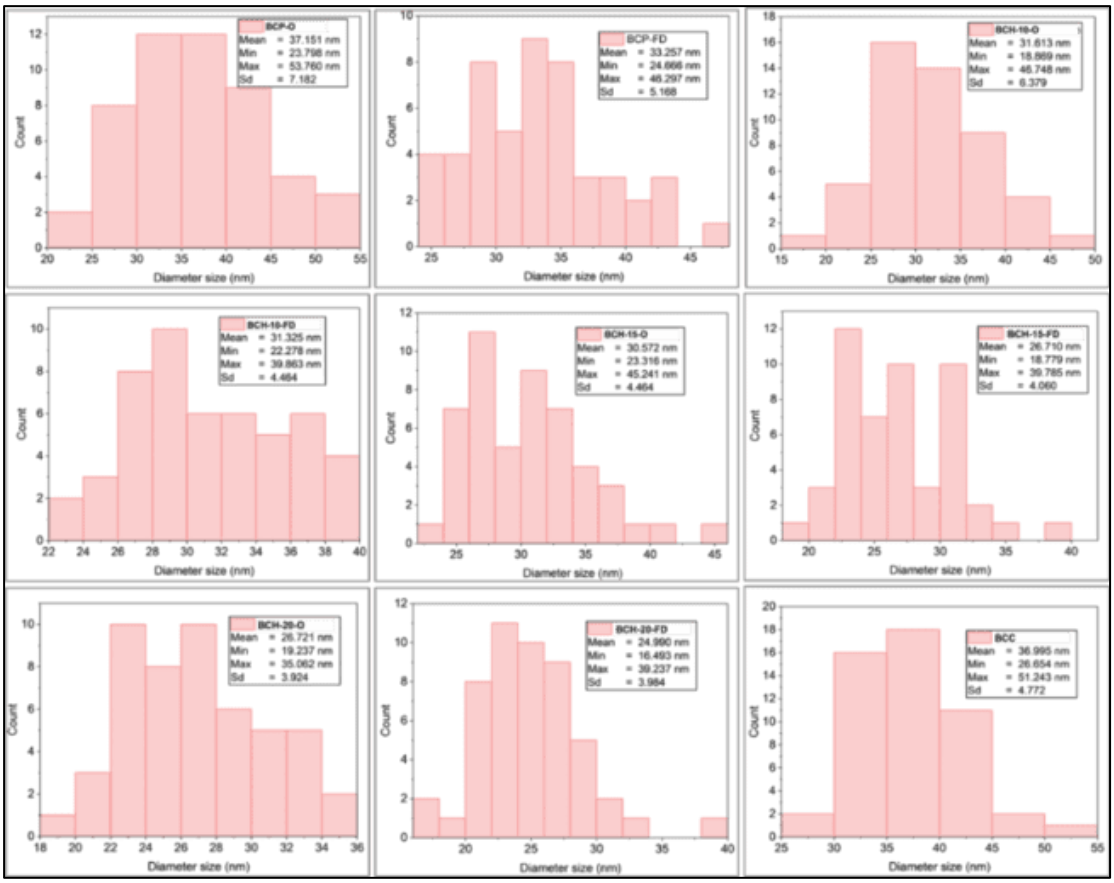

Figure 5.3 Fiber size distribution of BC-C, BCP, and microfluidized BC samples (BCH-10, BCH-15, and BCH-20), with "O" indicating oven-dried and "FD" indicating freeze-dried samples.

The BCC-O (control) and BCP-O samples have similar average fiber diameters of around 37 nm, while the BCP-FD sample is slightly smaller at 33.26 nm. As microfluidization intensity increases, the average fiber diameter decreases. The BCH-10-O and BCH-10-FD samples have average diameters of 31.61 nm and 31.33 nm, respectively. With stronger microfluidization, the diameters shrink further, with BCH-15-O and BCH-15-FD averaging 30.57 nm and 26.71 nm, respectively. The smallest diameters are in BCH-20-O and BCH-20-FD samples, with averages of 26.72 nm and 24.99 nm. Freeze-dried samples consistently have smaller fibers than oven-dried ones, indicating that the drying method affects fiber size. Standard deviations show less variation in fiber size with higher microfluidization, suggesting more uniform fiber sizes. The narrowing size range supports this trend.

The finding of this study is comparable with some of the previous studies. The HPH of 150 bar and 5 cycles effectively reduced the diameter of BC fiber size from a range of 75 to 100 nm into the range size of 30 to 35 nm (Sardjono et al. 2019). The HPH in 150 bar pressure decrease diameter of fiber size from 61.7±36.98 nm (control) to 53.24±27.05, 49.82±19.32, 47.2±15.34, and 46.38±17.18 nm for 5, 10, 15, and 20 cycles, respectively (Suryanto et al. 2021). This study indicates that microfluidization can effectively reduce the fiber size of BC, with freeze-drying resulting in more porous and smaller fibers compared to oven drying.

5.4.4 Fourier Transform Infrared Spectroscopy (FT-IR) Analysis

The FTIR spectra reveal slight differences among BC samples, including BCC, BCP, and microfluidized samples (BCH-10, BCH-15, BCH-20), with oven-dried (O) and freeze-dried (FD) treatments (**Figure 5.4(a, b, and c)**. A prominent band around 3430 and 3234 cm cm^{-1} corresponds to O–H stretching vibrations, indicating hydrogen bonding in the cellulose structure. The signal at approximately 2890 cm^{-1} arises from C–H stretching in CH_2 groups (Suryanto et al. 2021). Two distinct bands at 2360 and 2324 cm cm^{-1} suggest the presence of triple-bond functional groups, such as C≡C or C≡N, which may originate from polyphenols, organic compounds, proteins, yeast cells, or bacteria (Amarasekara et al. 2020; Srivastava and Mathur 2022). These bands were previously observed in BC produced with ethanol or sucrose-glucose combinations in the fermentation medium (reported in previous chapter). Similar findings have been reported in studies on nata de coco-derived BC, where residual proteins, nucleic acids, and microbial cells contributed to these signals (Fuller et al. 2018; Rachtanapun et al. 2021). The presence of these impurities in the BC matrix may be due to the thick and dense structure of the pellicle, which can impede their complete removal during the purification process.

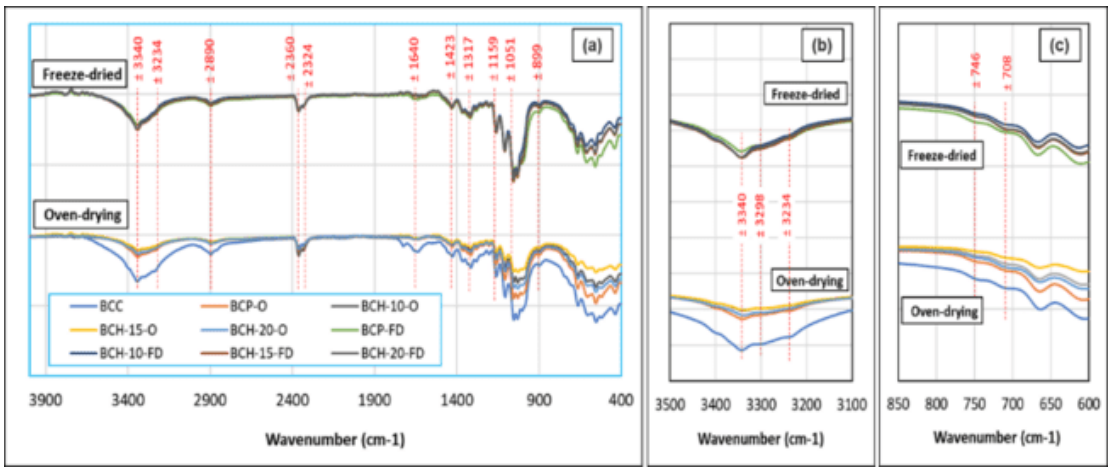

Figure 5.4 FTIR spectra of BC-C, BCP, and microfluidized BC samples (BCH-10, BCH-15, and BCH-20), with "O" indicating oven-dried and "FD" indicating freeze-dried samples

The band observed around 1640 cm^{-1} expressed the O-H signal of absorbed water (Suryanto et al. 2021). The band observed at 1427 cm^{-1} represents CH_2 symmetric bending, while the band at 1364 cm^{-1} corresponds to C-H symmetric bending (Fatima et al. 2023; Liu et al. 2023). In the fingerprint region between 1330 and 500 cm^{-1}, several distinct bands were observed, including those at approximately 1317, 1169, 1051, and 898 cm^{-1}. The band near 1317 cm^{-1} is associated with CH_2 wagging at the C-6 position (Liu et al. 2023) or could correspond to C–OH deformation vibrations (Wu et al. 2014). The band observed at 1051 cm^{-1} and 1028 cm^{-1} is associated with C-O-C stretching vibrations within the sugar ring (Liu et al. 2023). Additionally, the band at around 899cm^{-1} corresponds to C-O-C stretching in **β**-1,4-glycosidic linkages, signifying the presence of an amorphous absorption band (Ciolacu et al. 2011). The characteristic signals observed at 899 cm^{-1} and approximately 1423 cm^{-1} confirm that the samples are of cellulose type I (Kawee et al. 2018).

Mechanical treatment significantly impacts the FTIR spectral intensity of BC samples. The BCP and the BCH, processed using HPM, display a progressive reduction in peak sharpness and intensity compared to the untreated control sample (BCC). Prominent changes are observed in peaks around 3340 cm^{-1} (O–H stretching),

2890 cm^{-1} (C–H stretching), and 1159–1051 cm^{-1} (C–O–C and C–O stretching). Despite these intensity differences, the spectra retain the characteristic features of cellulose type I. The FTIR results indicate that although there is a slight reduction in transmittance peak intensity, the HPM process does not impact the chemical group of the BC sample. This result align with the previous finding (Kawee et al. 2018; Suryanto et al. 2021; Mohamad et al. 2022b).

The reduced intensity of the peaks at 3340 cm^{-1} and 3234 cm^{-1}, corresponding to hydroxyl group stretching vibrations, may result from the high pressure during HPM, which disrupts the cellulose network and induces defibrillation into nanofibrils (Kawee et al. 2018). The decrease in O–H bonding intensity is likely associated with the smaller fiber size, which limits the formation of extensive hydrogen bonding networks. The increased surface area exposes more hydroxyl groups that are not strongly bound within the network, further contributing to the observed reduction. These structural changes may lower the density of the crystalline structure, decreasing the number of O–H bonds. Additionally, smaller fibers are less capable of retaining bound water, which may also explain the reduced O–H stretching intensity observed in the spectra (Kawee et al. 2018).

The drying method significantly influences the intensity of the FTIR spectra of BC. In the 3000–3500 cm^{-1} region, corresponding to O–H stretching vibrations associated with hydrogen bonding in cellulose, freeze-dried samples exhibit sharper and more defined peaks compared to oven-dried ones. This suggests that freeze-drying affects the hydrogen bonding network differently, potentially preserving more hydroxyl groups in a less disrupted state. A similar phenomenon is observed in the 900–1200 cm^{-1} region, associated with C–O–C stretching and C–H deformation vibrations of the cellulose backbone. The more pronounced peaks in freeze-dried samples may indicate a looser, less compact structure with greater distances between cellulose macromolecules, leading to weaker hydrogen bonds (Zhang et al. 2011). These findings are consistent with previous studies (Zhang et al. 2011; Mohamad et al. 2022b).

5.4.5 X-Ray Diffraction (XRD) Analysis

The XRD patterns, (**Figure 5.5**), illustrate the effects of mechanical treatment, particularly HPM, and drying methods (oven-drying and freeze-drying) on the crystalline structure of BC. All the BC samples exhibit crystalline peaks characteristic of cellulose type I, with prominent reflections at 2θ values of ~14.56°, 16.72°, and 22.80°, corresponding to the (100), (010), and (110) crystallographic planes, respectively (Gaspar et al. 2014). The most intense peak, near 23°, is a defining feature of cellulose type I (Said Azmi et al. 2023; Hossen et al. 2024), confirming its crystalline structure (Samuel and Adefusika 2019). While the peak positions are consistent across samples, variations in their relative intensities and overall crystallinity indicate differences in cellulose chain orientation and structural properties (Said Azmi et al. 2023).

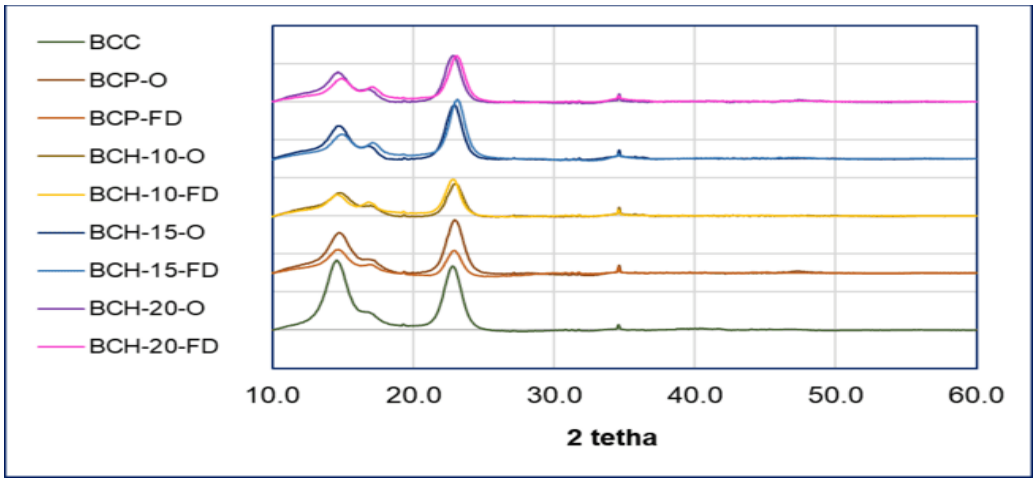

Figure 5.5 XRD spectra from the BC samples with different mechanical treatments and drying methods.

After mechanical treatments (BCP and BCH), a noticeable reduction in peak intensity and sharpness is observed, especially in BCH samples, indicating partial disruption of the crystalline structure. This disruption is attributed to defibrillation and fiber size reduction caused by HPM, which alters the ordered hydrogen bonding network in cellulose and lowers crystallinity (Kawee et al. 2018; Suryanto et al. 2021; Muhajir et al. 2022). Supporting data show that BCP and BCH samples have lower

crystallinity indices (CI) compared to the control (BCC), with BCH samples exhibiting progressively lower CI as the number of HPM cycles increases (Table 4). Previous studies align with these findings: the CI of BC and BCNFs after 10, 20, and 30 HPH cycles decreased from 85.65% to 76.99% (Kawee et al. 2018), while HPM pressures of 0–600 bar reduced CI from 87% to 70% (Muhajir et al. 2022). Similarly, BCNFs subjected to 5–20 HPH cycles at 150bar showed a CI decrease from 83% to 74% (Suryanto et al. 2021). These results confirm that increasing HPM intensity reduces the crystallinity of BC fibers.

Comparing the drying methods, freeze-dried samples (denoted by "-FD") exhibit broader and less intense peaks compared to oven-dried samples ("-O"). Freeze-drying appears to create a looser structure, possibly due to the sublimation of water, which minimizes compression and retains a more disordered arrangement of cellulose molecules. This aligns with the crystallinity index results, where freeze-dried samples generally have lower crystallinity compared to oven-dried counterparts (Zhang et al. 2011). Oven-drying, in contrast, may promote tighter packing of cellulose chains due to water removal under thermal conditions, preserving or even enhancing crystalline regions.

Further analysis of the XRD data reveals the average crystallite size of BC under various processing conditions, as summarized in **Table 5.4**. The data highlight the influence of HPM and drying methods on the crystalline structure of BC. Among the oven-dried samples, BCC (control) exhibits the largest crystallite size at 3.46 nm, indicating the crystalline domains remain largely undisturbed. In the case of BCP-O, the crystallite size decreases slightly to 3.41 nm, likely due to the blending processes. These treatments introduce mild mechanical forces, which may cause minor disruption to the crystalline regions without significant structural alteration. A more pronounced reduction in crystallite size is observed in BCH-10-O (3.08 nm), the lowest among oven-dried samples. This reduction is attributed to the mechanical shear forces exerted during 10 cycles of HPM, which fragment the cellulose fibrils and disrupt the crystalline

structure. Interestingly, additional HPM cycles (15 and 20) lead to an increase in crystallite size to 3.45 nm and 3.46 nm, respectively, nearly returning to the control value. This phenomenon suggests that extended mechanical treatment may promote reorganization or partial aggregation of cellulose chains during oven drying.

Table 5.4 Crystallinity index and average crystallite size of dried BC with various mechanical treatment and drying methods

Samples	Average Crystallite Size (nm)	Crystallinity Index (%)
BCC	3.46	86.33
BCP-O	3.41	82.73
BCP-FD	2.01	80.48
BCH-10-O	3.08	81.82
BCH-10-FD	2.16	74.69
BCH-15-O	3.45	78.75
BCH-15-FD	2.17	73.35
BCH-20-O	3.46	78.28
BCH-20-FD	2.14	71.82

For freeze-dried samples, the crystallite sizes are consistently smaller than oven-dried sample, highlighting the significant impact of the freeze-drying process on BC's crystalline structure. BCP-FD shows the smallest crystallite size (2.01 nm), indicating that the sublimation process during freeze drying disrupts hydrogen bonding and crystalline domains more effectively. BCH-10-FD, BCH-15-FD, and BCH-20-FD exhibit a slightly larger crystallite size (2.16 nm, 2.17 nm, and 2.14 nm, respectively) compared to BCP-FD, but it is still significantly smaller than oven-dried samples with little variation among them. This suggests that freeze drying limits the potential for chain reorganization regardless of the number of HPM cycles.

In summary, HPM reduces crystallite size by fragmenting fibrils, with the greatest reduction at 10 cycles (BCH-10). Beyond 10 cycles (15 and 20), some recovery

occurs during oven drying, likely due to chain reorganization. Freeze drying consistently produces smaller crystallites, as the sublimation process limits chain reorganization. The smallest crystallite size is in BCP-FD (2.01 nm), while BCH-10-O has the lowest crystallite size (3.08 nm) among oven-dried samples.

5.4.6 Thermogravimetric (TGA/DTG) Analysis

The TGA and DTG results in **Figure 5.6** and **Table 5.5** show how mechanical treatments and drying methods affect the thermal stability and decomposition of BC from Thai red tea kombucha. The control sample (BC-C), which was oven-dried without mechanical treatment, is used as a baseline for comparison. These results highlight the impact of different processes on the thermal behavior of BC.

Thermogravimetric analysis reveals that the thermal decomposition of BC occurs in two main stages. The first stage, occurring below 150°C, corresponds to the evaporation of moisture physically bound to the BC (Teixeira et al. 2019; Mohamad et al. 2022a). The second stage, spanning from 250°C to 600°C, involves the thermal degradation of cellulose, including the breakdown of glycosidic bonds, depolymerization, and the release of volatile compounds, followed by the oxidation of residual cellulose and **β**-glucan chains into carbonaceous char (Mohammadkazemi et al. 2015; Teixeira et al. 2019; Mohamad et al. 2022a). The effect of mechanical treatment, including HPM, appears minimal in samples subjected to oven drying (**Figure 5.6(a)**). Within these oven-dried samples, HPM cycles show only a subtle impact on peak degradation temperatures, with higher cycles causing slight shifts in the degradation profiles (**Figure 5.6(b)**). The first weight loss ranged from 4.68% to 5.69%, while the second weight loss ranged from 71.63% to 73.89%, leaving a residual weight between 21.23% and 22.82%. These findings are corroborated by the DTG analysis **(Figure 5.6(d)** and **(e)**), which shows that the maximum degradation temperatures (DTG max) for all oven-dried samples are within a comparable range of approximately 275–385°C. The DTG T_{Max} values are closely clustered, spanning from

341.67°C to 343.67°C. Compared to freeze-dried samples (e.g., BC-P-FD and BC-HPM10-FD), which exhibit higher DTG T_{Max} values (ranging from 356°C to 371.17°C), oven-dried samples (e.g., BC-P-O and BC-HPM10-O) demonstrate slightly lower peak thermal stability. However, oven-dried samples exhibit higher onset degradation temperatures, likely due to their denser structure, which may provide greater resistance to initial decomposition.

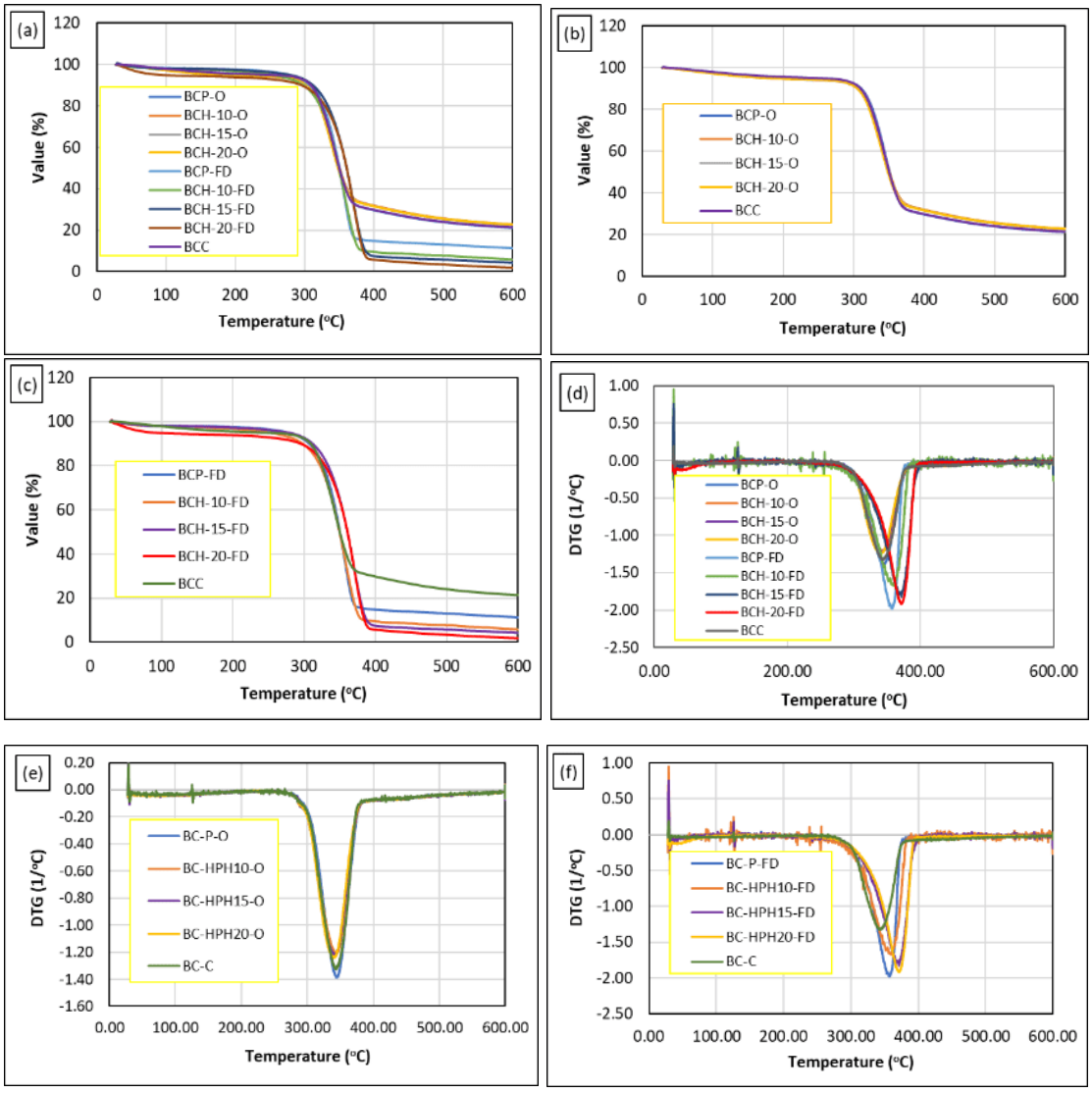

Figure 5.6 TGA (a) and DSC (b) results of dried BC from optimized RTC kombucha with various treatments and drying methods.

Table 5.5 Detail parameter of TGA/DTG analysis of BC samples with different mechanical treatments and drying methods

Samples	First stage weight loss (%)	Second stage weight loss (%)	Residue (%)	DTG Peak range (°C)	DTG T_{Max} (°C)
BCC	4.68	73.86	21.43	275 – 385	342.67
BCP-O	4.86	73.89	21.23	275 – 385	343.67
BCP-FD	2.80	85.80	11.31	285 - 382	356.67
BCH-10-O	5.52	71.63	22.82	275 – 385	343.17
BCH-10-FD	3.55	90.46	5.85	265 - 385	359.17
BCH-15-O	5.69	71.76	22.53	275 – 385	342.17
BCH-15-FD	3.09	92.55	4.25	266 - 403	371.17
BCH-20-O	5.59	71.77	22.73	275 – 385	341.67
BCH-20-FD	6.53	91.50	1.93	265 - 399	371.17

In contrast, samples prepared using freeze-drying methods show more varied TGA and DTG results across all samples. Mechanical treatments significantly influence these analysis results. Microfluidized BC samples (BCH-10-FD, BCH-15-FD, BCH-20-FD) exhibit higher weight loss during the second stage of decomposition and leave less residual material after cellulose decomposition at 600°C (Figure 6(a)). As the number of HPM cycles increases, the weight loss becomes greater, and the residual values decrease (Figure 6(c)). The DTG profiles of freeze-dried samples vary considerably, with peak temperatures ranging from approximately 265°C to 403°C. The DTG T_{Max} values for these samples fall between 356°C and 371.17°C, which are relatively higher than those of oven-dried samples. While freeze-dried samples are more porous, their DTG T_{Max} values indicate that they can exhibit higher peak degradation temperatures than oven-dried samples. This suggests that while porosity might accelerate degradation under direct flame exposure, the intrinsic stability of the material in controlled thermal analysis may be slightly better due to structural

modifications. Freeze-dried samples also display sharper DTG peaks compared to oven-dried samples, suggesting a faster degradation rate due to their porous structure resulting in a lower effect of flame retardant (Dai et al. 2018; Mohamad et al. 2022b). The porous structure is a result of sublimation during the freeze-drying process. Overall, freeze-drying combined with mechanical treatments reduces the thermal stability of BC compared to oven drying.

5.5 Conclusion

This study demonstrates that mechanical treatment, particularly high-pressure microfluidization (HPM), plays a critical role in modifying the physicochemical, structural, and thermal properties of bacterial cellulose (BC). HPM treatment led to a significant decrease in moisture content and water holding capacity (WHC), likely due to the disruption of the cellulose fiber network. Notably, the highest WHC was observed in the untreated BC (96.58 ± 13.91 g water/g cellulose), whereas microfluidized samples exhibited markedly lower capacities.

Increasing HPM cycles resulted in reduced fiber diameters, from 37 nm in the control to 24.99 nm in the most treated samples. The method of drying also influenced BC morphology: freeze-drying produced finer fibrils and enhanced porosity, while oven drying led to denser structures. Particle size analysis confirmed that HPM generated smaller and more uniform particles, although PDI and zeta potential values indicated moderate stability due to partial re-aggregation.

Structural modifications were supported by SEM and XRD analyses, revealing distinct morphological and crystallinity shifts depending on treatment intensity and drying method. Thermal analysis further confirmed that freeze-dried BC, despite being more porous, demonstrated higher degradation temperatures (DTG T_{max} 341.67°C–371.17°C) than oven-dried counterparts.

In conclusion, the combination of HPM and appropriate drying techniques offers a versatile approach to tailoring BC characteristics. These modifications are

crucial for expanding BC's potential in various industrial applications, particularly where specific structural and thermal attributes are required.

5.6 References

Amarasekara AS, Wang D, Grady TL (2020) A comparison of kombucha SCOBY bacterial cellulose purification methods. SN Appl Sci 2:1–7. https://doi.org/10.1007/s42452-020-1982-2

Andree V, Niopek D, Müller C, et al (2021) Influence of drying methods on the physical properties of bacterial nanocellulose. Mater Res Express 8:. https://doi.org/10.1088/2053-1591/abe016

Aswini K, Gopal NO, Uthandi S (2020) Optimized culture conditions for bacterial cellulose production by Acetobacter senegalensis MA1. BMC Biotechnol 20:1–16. https://doi.org/10.1186/s12896-020-00639-6

Balistreri GN, Campbell IR, Li X, et al (2024) Bacterial cellulose nanoparticles as a sustainable drug delivery platform for protein-based therapeutics. RSC Appl Polym 2:172–183. https://doi.org/10.1039/d3lp00184a

Betlej I, Salerno-Kochan R, Jankowska A, et al (2021) The impact of the mechanical modification of bacterial cellulose films on selected quality parameters. Coatings 11:1–12. https://doi.org/10.3390/coatings11111275

Choi SM, Rao KM, Zo SM, Shin EJ (2022) Bacterial Cellulose and Its Applications. Polymers (Basel) 14:1–44. https://doi.org/https://doi.org/10.3390/polym14061080

Ciolacu D, Ciolacu F, Popa VI (2011) Amorphous cellulose - Structure and characterization. Cellul Chem Technol 45:13–21

Dai H, Ou S, Huang Y, Huang H (2018) Utilization of pineapple peel for production of nanocellulose and film application. Cellulose 25:1743–1756. https://doi.org/10.1007/s10570-018-1671-0

Danaei M, Dehghankhold M, Ataei S, et al (2018) Impact of particle size and

polydispersity index on the clinical applications of lipidic nanocarrier systems. Pharmaceutics 10:1–17. https://doi.org/10.3390/pharmaceutics10020057

Dima SO, Panaitescu DM, Orban C, et al (2017) Bacterial nanocellulose from side-streams of kombucha beverages production: Preparation and physical-chemical properties. Polymers (Basel) 9:. https://doi.org/10.3390/polym9080374

Fang L, Catchmark JM (2014) Structure characterization of native cellulose during dehydration and rehydration. Cellulose 21:3951–3963. https://doi.org/10.1007/s10570-014-0435-8

Fatima A, Ortiz-Albo P, Neves LA, et al (2023) Biosynthesis and characterization of bacterial cellulose membranes presenting relevant characteristics for air/gas filtration. J Memb Sci 674:. https://doi.org/10.1016/j.memsci.2023.121509

Fuller ME, Andaya C, McClay K (2018) Evaluation of ATR-FTIR for analysis of bacterial cellulose impurities. J Microbiol Methods 144:145–151. https://doi.org/10.1016/j.mimet.2017.10.017

Gaspar D, Fernandes SN, De Oliveira AG, et al (2014) Nanocrystalline cellulose applied simultaneously as the gate dielectric and the substrate in flexible field effect transistors. Nanotechnology 25:. https://doi.org/10.1088/0957-4484/25/9/094008

Gayathry G, Gopalaswamy G (2014) Production and characterisation of microbial cellulosic fibre from Acetobacter xylinum. Indian J Fibre Text Res 39:93–96

Guo X, Chen M, Li Y, et al (2020) Modification of food macromolecules using dynamic high pressure microfluidization: A review. Trends Food Sci Technol 100:223–234. https://doi.org/10.1016/j.tifs.2020.04.004

Hossen MT, Kundu CK, Pranto BRR, et al (2024) Synthesis, characterization, and cytotoxicity studies of nanocellulose extracted from okra (Abelmoschus Esculentus) fiber. Heliyon 10:e25270. https://doi.org/10.1016/j.heliyon.2024.e25270

Hussain Z, Sajjad W, Khan T, Wahid F (2019) Production of bacterial cellulose from industrial wastes: a review. Cellulose 26:2895–2911

Kawee N, Lam NT, Sukyai P (2018) Homogenous isolation of individualized bacterial nanofibrillated cellulose by high pressure homogenization. Carbohydr Polym 179:394–401. https://doi.org/10.1016/j.carbpol.2017.09.101

Li P, Wang Y, Hou Q, et al (2020) Preparation of cellulose nanofibrils from okara by high pressure homogenization method using deep eutectic solvents. Cellulose 27:2511–2520. https://doi.org/10.1007/s10570-019-02929-5

Liu X, Cao L, Wang S, et al (2023) Isolation and characterization of bacterial cellulose produced from soybean whey and soybean hydrolyzate. Sci Rep 13:1–10. https://doi.org/10.1038/s41598-023-42304-w

Mert ID (2020) The applications of microfluidization in cereals and cereal-based products: An overview. Crit Rev Food Sci Nutr 60:1007–1024. https://doi.org/10.1080/10408398.2018.1555134

Mohamad S, Abdullah LC, Jamari SS, et al (2022a) Influence of drying method on the crystal structure and thermal property of oil palm frond juice-based bacterial cellulose. J Mater Sci 57:1462–1473. https://doi.org/10.1007/s10853-021-06685-5

Mohamad S, Abdullah LC, Jamari SS, et al (2022b) Production and Characterization of Bacterial Cellulose Nanofiber by Acetobacter Xylinum 0416 Using Only Oil Palm Frond Juice as Fermentation Medium. J Nat Fibers 19:16005–16016. https://doi.org/10.1080/15440478.2022.2140243

Mohammadkazemi F, Azin M, Ashori A (2015) Production of bacterial cellulose using different carbon sources and culture media. Carbohydr Polym 117:518–523. https://doi.org/10.1016/j.carbpol.2014.10.008

Muhajir M, Suryanto H, Pradana YRA, Yanuhar U (2022) Effect of Homogenization Pressure on Bacterial Cellulose Membrane Characteristic Made from Pineapple Peel Waste. J Mech Eng Sci Technol 6:34. https://doi.org/10.17977/um016v6i12022p034

Nurfadila N, Maddu A, Winarti C, Kurniati M (2019) Cellulose-based nano hydrogel from corncob by gamma irradiation. IOP Conf Ser Earth Environ Sci 299:.

https://doi.org/10.1088/1755-1315/299/1/012003

R. Rebelo A, Archer AJ, Chen X, et al (2018) Dehydration of bacterial cellulose and the water content effects on its viscoelastic and electrochemical properties. Sci Technol Adv Mater 19:203–211. https://doi.org/10.1080/14686996.2018.1430981

Rachtanapun P, Jantrawut P, Klunklin W, et al (2021) Carboxymethyl bacterial cellulose from nata de coco: Effects of NaOH. Polymers (Basel) 13:1–17. https://doi.org/10.3390/polym13030348

Said Azmi SNN, Samsu Z 'Asyiqin, Mohd Asnawi ASF, et al (2023) The production and characterization of bacterial cellulose pellicles obtained from oil palm frond juice and their conversion to nanofibrillated cellulose. Carbohydr Polym Technol Appl 5:100327. https://doi.org/10.1016/j.carpta.2023.100327

Samuel OS, Adefusika AM (2019) Influence of Size Classifications on the Structural and Solid-State Characterization of Cellulose Materials. In: Pascual R, Martín MEE (eds) Cellulose. IntechOpen

Sardjono SA, Suryanto H, Aminnudin, Muhajir M (2019) Crystallinity and morphology of the bacterial nanocellulose membrane extracted from pineapple peel waste using high-pressure homogenizer. In: AIP Conference Proceedings. AIP Publishing, pp 080015-1-080015–5

Srivastava S, Mathur G (2022) Komagataeibacter saccharivorans strain BC-G1: an alternative strain for production of bacterial cellulose. Biologia (Bratisl) 77:3657–3668. https://doi.org/10.1007/s11756-022-01222-4

Suryanto H, Muhajir M, Susilo BD, et al (2021) Nanofibrillation of bacterial cellulose using high-pressure homogenization and its films characteristics. J Renew Mater 9:1717–1728. https://doi.org/10.32604/jrm.2021.015312

Teixeira SRZ, Dos Reis EM, Apati GP, et al (2019) Biosynthesis and functionalization of bacterial cellulose membranes with cerium nitrate and silver nanoparticles. Mater Res 22:1–13. https://doi.org/10.1590/1980-5373-MR-2019-0054

Tomkowiak K, Mazela B, Szubert Z, Perdoch W (2024) Hydrophobic Cellulose-Based

Sorbents for Oil/Water Separation. Molecules 29:. https://doi.org/10.3390/molecules29194661

Wang H, Zuo M, Ding N, et al (2019) Preparation of Nanocellulose with High-Pressure Homogenization from Pretreated Biomass with Cooking with Active Oxygen and Solid Alkali. ACS Sustain Chem Eng 7:9378–9386. https://doi.org/10.1021/acssuschemeng.9b00582

Wang Y, Wei X, Li J, et al (2015) Study on nanocellulose by high pressure homogenization in homogeneous isolation. Fibers Polym 16:572–578. https://doi.org/10.1007/s12221-015-0572-1

Widyastuti FK, Kartika Fitri AC (2023) Optimization Production and Characterization of Bacterial Cellulose from Cornhusk. CHEESA Chem Eng Res Artic 6:49. https://doi.org/10.25273/cheesa.v6i1.11781.49-55

Wu LM, Tong DS, Zhao LZ, et al (2014) Fourier transform infrared spectroscopy analysis for hydrothermal transformation of microcrystalline cellulose on montmorillonite. Appl Clay Sci 95:74–82. https://doi.org/10.1016/j.clay.2014.03.014

Yan H, Chen X, Li J, et al (2016) Synthesis of alginate derivative via the Ugi reaction and its characterization. Carbohydr Polym 136:757–763. https://doi.org/10.1016/j.carbpol.2015.09.104

Yanti NA, Ahmad SW, Muhiddin NH (2018) Evaluation of inoculum size and fermentation period for bacterial cellulose production from sago liquid waste. J Phys Conf Ser 1116:. https://doi.org/10.1088/1742-6596/1116/5/052076

Yilmaz M, Goksungur Y (2024) Optimization of Bacterial Cellulose Production from Waste Figs by Komagataeibacter xylinus. Fibers 12:1–18. https://doi.org/10.3390/fib12030029

Zhai X, Lin D, Li W, Yang X (2020) Improved characterization of nanofibers from bacterial cellulose and its potential application in fresh-cut apples. Int J Biol Macromol 149:178–186. https://doi.org/10.1016/j.ijbiomac.2020.01.230

Zhang CJ, Wang L, Zhao JC, Zhu P (2011) Effect of drying methods on structure and mechanical properties of bacterial cellulose films. Adv Mater Res 239–242:2667–2670. https://doi.org/10.4028/www.scientific.net/AMR.239-242.2667

Zhong C (2020) Industrial-Scale Production and Applications of Bacterial Cellulose. Front. Bioeng. Biotechnol. 8:1–19